Integral Cycle Mode Control of the Series Resonant Converter

GYU B. JOUNG, CHUN T. RIM, AND GYU H. CHO

Abstract—**A new control method for the series resonant converter (SRC) in which the device switching instants are always synchronized to the zero crossing points of the resonant current is proposed. Output voltage is controlled by proper selection of the switch modes by varying the duty ratio of powering mode and free resonant mode. Each switch mode is analyzed and the dc transfer function is obtained. It is also shown that the simulation results coincide well with the practical case. The SRC with the proposed control scheme shows many advantages, such as low current switching stress, low switching loss, low electromagnetic interference, high input power factor, and wide control range. Some of these characteristics are verified experimentally.**

I. Introduction

RESONANT converters are becoming widely used in industrial and aerospace applications due to their numerous merits [1]–[9]. Conventional series resonant converters (SRC's) can be classified into two schemes according to the control method. One is the frequency domain control scheme, and the other is the phase domain control scheme. In the frequency domain control scheme, the output voltage is controlled by the ratio of the switching frequency and the circuit resonant frequency [1]–[5], [7], [8]. On the other hand, in the phase domain control scheme, it is achieved by the phase difference between two inverters where the switching frequency of each converter is fixed to the resonant frequency [9].

In the frequency domain control scheme, the output voltage depends largely on the load condition as well as the switching frequency, which makes it difficult to control the system properly [7]. In particular, the control range of the output voltage becomes narrow for light load operation, and the device current switching stress becomes severe when the switching frequency deviates from the resonant frequency [6]. The phase domain control scheme is more advantageous than the frequency domain control scheme in terms of the load independency. However, this scheme also undergoes severe current switching stress as phase difference becomes large [9].

It is well-known that the SRC operates optimally when the switching frequency exactly coincides with the resonant frequency. The output voltage cannot be controlled, however, so far as the frequency and phase are fixed. Therefore, a time domain control method is suggested in this paper to adjust the output voltage still satisfying its optimum operating conditions.

This proposed control scheme has inherent advantages such as zero current switching stress, low switching loss, low electromagnetic interference (EMI), and wide control range. Switch modes are analyzed for an SRC with MOSFET, and a practical control scheme is suggested and verified experimentally.

Manuscript received February 8, 1988; revised August 18, 1988. This paper was presented at the 1988 IEEE Power Electronics Specialists Conference, Kyoto, Japan, April 11–14.

The authors are with the Department of Electrical Engineering, Korea Advanced Institute of Science and Technology, P.O. Box 150, Chongyang, Seoul 130-650, Korea.

IEEE Log Number 8824728.

II. Operating Modes and Control Method of SRC

A. Operating Modes

The basic power circuit topology of the SRC is shown in Fig. 1. The power circuit has four switch modes as shown in Fig. 2: the powering mode, the free resonant mode, the regeneration mode, and the discontinuous mode. These modes are classified according to the direction of power flow. Switch on/off control always occurs in synchronization with the current zero crossing points.

Denoting the circuit quantities as input voltage V_s, output voltage v_o, inductor current i_L, capacitor voltage v_c, and the resonant tank circuit and load parameters ω_r, Z, and Q which are

$$\omega_r = \frac{1}{\sqrt{LC}} \tag{1}$$

$$Z = \sqrt{L/C} \tag{2}$$

$$Q = \omega_r L/R, \tag{3}$$

the description of each mode is as follows.

1) Powering Mode: S1,S4 and S2,S3 pairs are turned on and off alternately in synchronization with the current zero crossings. The applied voltage v_s across the tank circuit and the resonant current i_L are in phase as shown in Fig. 3(a). During this mode, the source power is delivered to the LC tank including the load.

2) Free Resonant Mode: D2,S4 and S2,D4 pairs (or, equivalently, D1,S3 and S1,D3 pairs) are turned on and off alternately. In this mode, power is not supplied to the tank circuit while the sinusoidal resonant current free-runs and gradually decreases as shown in Fig. 3(b). In this mode, the LC tank energy is delivered in the load.

3) Regeneration Mode: All of the forced commutation switches (S1–S4) are turned off. Instead, the D1,D4 and

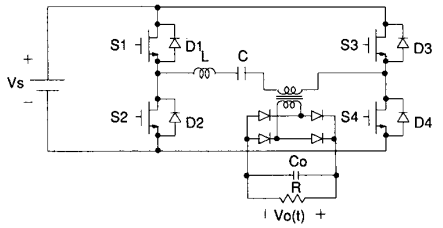

Fig. 1. Power circuit topography of SRC.

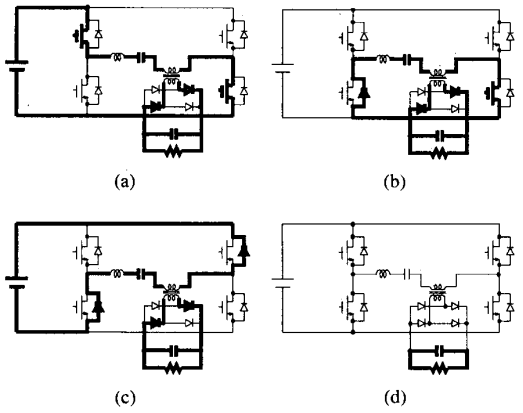

Fig. 2. Four modes of SRC operation. (a) Powering mode. (b) Free resonant mode. (c) Regeneration mode. (d) Discontinuous mode.

D2,D3 pairs are alternately turned on and off in synchronization with the resonant current. During this mode, the applied voltage across the tank circuit and resonant current are out of phase, so the resonant current decreases faster than the current of the free resonant mode. As shown in Fig. 3(c), the *LC* tank energy is returned to the source while transferring part of the energy to the load.

4) Discontinuous Mode: As the previous free resonant or regeneration mode goes on, the tank resonant current decreases, and it can reach zero, as shown in Fig. 3(d), without any energy stored in the *LC* tank.

From these characteristics, the operation modes are summarized in Table I.

B. Mode Control Methods

The output voltage of SRC can be controlled by moderate selection of the four modes. Mode selection is allowed only at current zero crossing points, thus the mode interval length should be an integer multiple of half cycles of the resonant frequency. In this sense, it is called the *integral cycle mode control scheme*. The diagram of the time domain control scheme is shown in Fig. 4. In this diagram, powering, free resonant, and regeneration modes are selectable by switches S1–S4. Thus these modes are controllable except the discontinuous mode because the discontinuous mode occurs independently of the external switches.

The powering mode increases the output voltage, whereas the free resonant and regeneration modes decrease it. Thus the output voltage can be controlled by

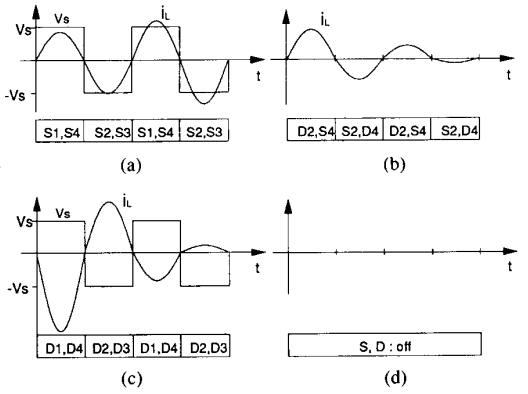

Fig. 3. Tank circuit waveforms i_L v_s of each mode. (a) Powering mode. (b) Free resonant mode. (c) Regeneration mode. (d) Discontinuous mode.

properly combining the powering mode and either the free resonant or the regeneration modes. Comparing the two passive modes, the regeneration mode deteriorates the input power factor, thus it is undesirable to include this mode in the control scheme. Therefore, the powering and free resonant modes with (or without) the discontinuous mode are used for the output voltage control in this paper. Fig. 5 briefly illustrates the waveforms of the proposed control scheme. In this control scheme, the output voltage is regulated by the duty ratio of the powering mode and free resonant mode with (or without) discontinuous mode. As the duty ratio increases, the output voltage is also increased.

III. Analysis of the Proposed Control Scheme

The equations for analyzing the resonant operation are shown in the Appendix for the four respective modes. However, exact analysis takes a long time, and understanding the time domain control characteristics is very difficult.

For simplicity, the operation modes of the SRC can be approximately analyzed by the low ripple approximation method [4] because the output filter capacitor C_o is sufficiently larger than the tank circuit capacitor C in the practical case. To apply the low ripple approximation method, all variables during the kth resonant period, $kT/2 \le t < (k+1)T/2$ are denoted by index k. As indicated in Fig. 6, $v_o(k)$ is the output voltage, $v_c(k)$ is the tank capacitor voltage at the switching instant, and $i_p(k)$ is the peak current during the kth event.

Because the magnitude of the capacitor voltage is related to the stored energy of the capacitor and the magnitude of the inductor current is also related to the stored energy of the inductor, we can change the variables $v_c(k)$, $i_p(k)$ into new variables $v_c^*(k)$, $i_p^*(k)$, where

$$v_c^*(k) = |v_c(k)| \tag{4}$$

$$i_p^*(k) = |i_p(k)| \tag{5}$$

and assuming that $C_o \gg C$, then the discrete state equa-

TABLE I
CHARACTERISTICS OF EACH MODE

Operation Modes	Tank Circuit Variables				
	Voltage	Current	Input Power P_i	Output Power P_o	$P_i - P_o$
Powering mode	$\pm V_s$	$\pm\lvert i_L(t)\rvert$	$V_s \cdot \lvert i_L(t)\rvert$	$v_o \cdot \lvert i_L(t)\rvert$	$(V_s - v_o) \cdot \lvert i_L(t)\rvert$
Free resonant mode	0	$\pm\lvert i_L(t)\rvert$	0	$v_o \cdot \lvert i_L(t)\rvert$	$-v_o \cdot \lvert i_L(t)\rvert$
Regeneration mode	$\mp V_s$	$\pm\lvert i_L(t)\rvert$	$-V_s \cdot \lvert i_L(t)\rvert$	$v_o \cdot \lvert i_L(t)\rvert$	$-(V_s + v_o) \cdot \lvert i_L(t)\rvert$
Discontinuous mode	0	0	0	0	0

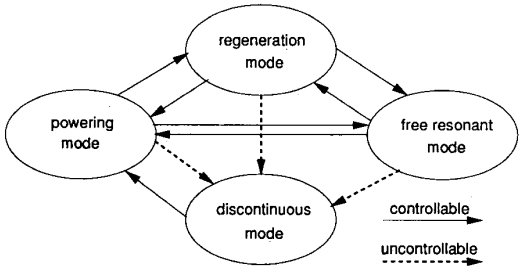

Fig. 4. Diagram of time domain control scheme.

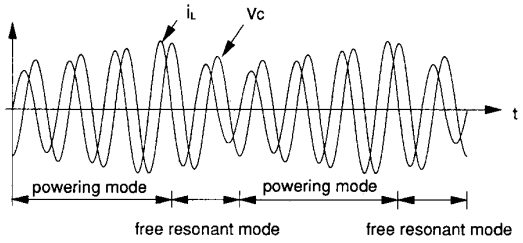

Fig. 5. Typical inductor current and capacitor voltage waveforms in proposed integral cycle mode control.

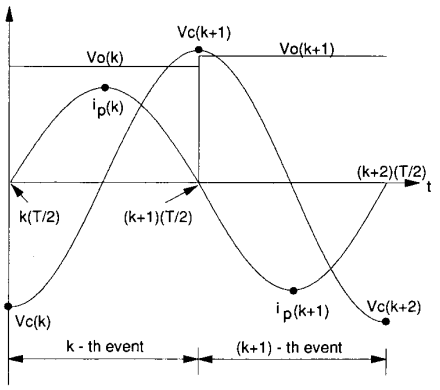

Fig. 6. Representation of events.

tions of the four operating modes can be written using the low ripple approximation method as follows.

1) Powering Mode: During the kth resonant interval, the output voltage is assumed to be nearly constant: that is, $v_o(t) \cong v_o(k)$. Since the inductor current and the capacitor voltage change sinusoidally, the kth capacitor voltage and output voltage can be evaluated as follows:

$$v_c^*(k+1) = \frac{1}{CZ}\int_{kT/2}^{kT/2+T/2} [v_c^*(k) + V_s - v_o(k)] \cdot \sin\{\omega_r(t - kT/2)\}\, dt - v_c^*(k) \quad (6)$$

$$v_o(k+1) = \frac{1}{C_oZ}\int_{kT/2}^{kT/2+T/2} [v_c^*(k) + \{V_s - v_o(k)\}] \cdot \sin\{\omega_r(t - kT/2)\}\, dt + v_o^*(k) - \frac{1}{C_o}\int_{kT/2}^{kT/2+T/2} \frac{v_o(k)}{R}\, dt \quad (7)$$

where, $T = 2\pi\sqrt{LC}$.

From (6) and (7), the state equation during the powering mode can be given as

$$\begin{bmatrix} v_c^*(k+1) \\ v_o(k+1) \end{bmatrix} = \begin{bmatrix} 1 & -2 \\ \delta & 1 - \delta - \delta^* \end{bmatrix} \begin{bmatrix} v_c^*(k) \\ v_o(k) \end{bmatrix} + \begin{bmatrix} 2 \\ \delta \end{bmatrix} V_s \quad (8)$$

$$i_p^*(k) = \frac{v_c^*(k) + V_s - v_o(k)}{Z} \quad (9)$$

where

$$\delta = 2\frac{C}{C_o} \qquad \delta^* = \frac{\pi}{2}Q\delta.$$

2) Free Resonant Mode: In this mode, all conditions are equal to those of the powering mode except V_s being set to zero. Therefore, we can easily obtain the following state equation from (8) and (9):

$$\begin{bmatrix} v_c^*(k+1) \\ v_o(k+1) \end{bmatrix} = \begin{bmatrix} 1 & -2 \\ \delta & 1 - \delta - \delta^* \end{bmatrix} \begin{bmatrix} v_c^*(k) \\ v_o(k) \end{bmatrix} \quad (10)$$

$$i_p^*(k) = \frac{v_c^*(k) - v_o(k)}{Z}. \quad (11)$$

3) Regeneration Mode: In this mode, all of the conditions are equal to those of the powering mode except that V_s is changed into $-V_s$. Therefore, we can obtain the following equations from (8) and (9) as

$$\begin{bmatrix} v_c^*(k+1) \\ v_o(k+1) \end{bmatrix} = \begin{bmatrix} 1 & -2 \\ \delta & 1 - \delta - \delta^* \end{bmatrix} \begin{bmatrix} v_c^*(k) \\ v_o(k) \end{bmatrix} + \begin{bmatrix} -2 \\ -\delta \end{bmatrix} V_s \quad (12)$$

$$i_p^*(k) = \frac{v_c^*(k) - V_s + v_o(k)}{Z}. \quad (13)$$

4) Discontinuous Mode: From (A4) and $v_c^*(k+1) = v_c^*(k)$ in event k, we obtain

$$\begin{bmatrix} v_c^*(k+1) \\ v_o(k+1) \end{bmatrix} = \begin{bmatrix} 1 & 0 \\ 0 & 1-\delta^* \end{bmatrix} \begin{bmatrix} v_c^*(k) \\ v_o(k) \end{bmatrix} \quad (14)$$

$$i_p^*(k) = 0. \quad (15)$$

A. DC Transfer Function

Assume that the interval length of the powering mode is $m(T/2)$ out of the total period $n(T/2)$ as shown in Fig. 7, the dc transfer function can be given as functions of m and n. If the new variables are defined as

$$x_1(k) = v_c^*(k) \quad (16a)$$

$$x_2(k) = v_o(k) \quad (16b)$$

$$x(k) = \begin{bmatrix} x_1(k) \\ x_2(k) \end{bmatrix} \quad (16c)$$

and if the converter is operated in the continuous mode, then the mth state during the powering mode are found from (8) as

$$\boldsymbol{x}(k+1) = \boldsymbol{A}\boldsymbol{x}(k) + \boldsymbol{B}V_s$$

$$\boldsymbol{x}(k+2) = \boldsymbol{A}^2\boldsymbol{x}(k) + (\boldsymbol{A}\boldsymbol{B} + \boldsymbol{B})V_s$$

$$\vdots$$

$$\boldsymbol{x}(k+m) = \boldsymbol{A}^m\boldsymbol{x}(k) + \sum_{i=1}^{m} (\boldsymbol{A}^{i-1}\boldsymbol{B})V_s \quad (17)$$

where

$$\boldsymbol{A} = \begin{bmatrix} 1 & -2 \\ \delta & 1-\delta-\delta^* \end{bmatrix} \qquad \boldsymbol{B} = \begin{bmatrix} 2 \\ \delta \end{bmatrix}. \quad (18)$$

During the free resonant mode, the state equations can be evaluated by (10) as

$$\boldsymbol{x}(k+n) = \boldsymbol{A}^{n-m}\boldsymbol{x}(k+m). \quad (19)$$

From (17) and (19), we obtain

$$\boldsymbol{x}(k+n) = \boldsymbol{A}^n\boldsymbol{x}(k) + \boldsymbol{A}^{n-m} \sum_{i=1}^{m} (\boldsymbol{A}^{i-1}\boldsymbol{B})V_s. \quad (20)$$

In the steady state, it is reasonable to assume that

$$\boldsymbol{x}(k) = \boldsymbol{x}(k+n). \quad (21)$$

Therefore, $\boldsymbol{x}(k)$ is determined as follows:

$$\boldsymbol{x}(k) = (\boldsymbol{I} - \boldsymbol{A}^n)^{-1}\boldsymbol{A}^{n-m} \sum_{i=1}^{m} (\boldsymbol{A}^{i-1}\boldsymbol{B})V_s \quad (22)$$

where $\boldsymbol{I}$ is an identity matrix. Finally, the transfer function G_v is given by

$$G_v = v_o/V_s = C\boldsymbol{x}(k)$$

$$= \boldsymbol{C}(\boldsymbol{I} - \boldsymbol{A}^n)^{-1}(\boldsymbol{A}^{n-m}) \sum_{i=1}^{m} (\boldsymbol{A}^{i-1}\boldsymbol{B}). \quad (23)$$

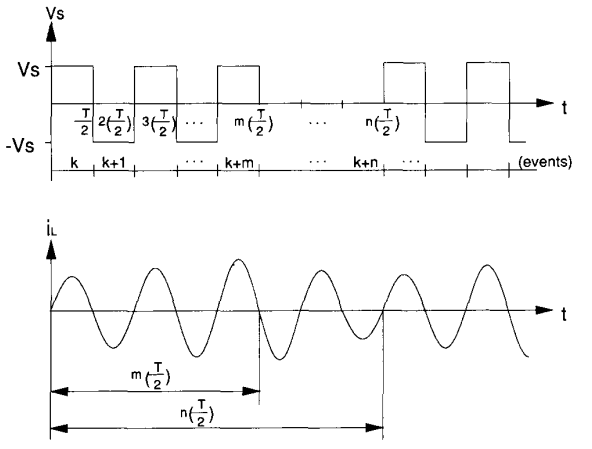

Fig. 7. Voltage (v_s) and current (i_L) waveforms of tank circuit for duty ratio of m/n.

From (23), the transfer function G_v is found to be dependent on Q, C/C_o, m, and n. If $Q \gg 1$, we see from Fig. 8 that the output voltage is directly proportional to the duty ratio m/n. Note that the output voltage can be controlled in a wide range from zero to the maximum. However, the output voltage level is discrete and the number of discrete levels are n. To control the output voltage by m, the step voltage should be given by V_s/n. Thus to reduce the incremental step of the output voltage, the number of n should be increased.

Fig. 9 shows the transfer function for different values of Q and n. We can see from this curve that the dc transfer function deviates from the straight line as Q and m decreases and n increases. This is due to the discontinuous mode. When Q is small, the LC tank energy also becomes small and the tank current fastly reduces to zero and becomes discontinuous mode. When the duty ratio m/n is small, the energy dissipation interval of LC tank becomes longer than the energy storage interval, and thus the discontinuous mode appears. When the discontinuous mode appears, the dc transfer function curve becomes nonlinear. In practice, however, the nonlinearity can be eliminated by feedback control.

Fig. 10 shows the dc transfer function as a function of load R for three selected values of m for $n = 5$. We can see that the output voltage does not depend on the load so far as R is smaller than a certain value. As R becomes larger than the critical value, the output voltage becomes high because the discontinuous mode appears. From this figure, the Q range can be determined for a given linear region if the load and the output voltage are given.

B. Time Domain Simulation for the Feedback Control Scheme

Fig. 11 shows the control scheme used for the experiment. In this figure, the duty ratio of the powering mode and the free resonant mode with (or without) the discontinuous mode is controlled by the time domain selection of the switch modes from the difference signal between

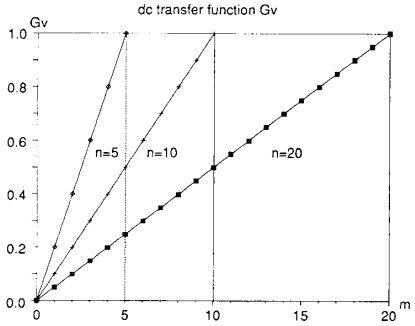

Fig. 8. DC transfer function of continuous resonant current switch modes.

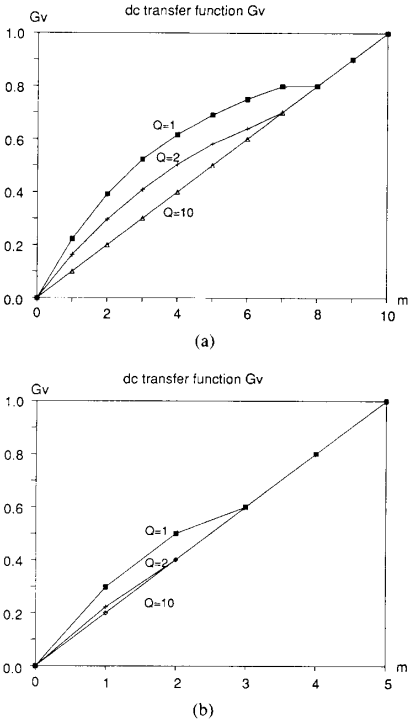

Fig. 9. DC transfer function for different Q and n values. (a) $n = 10$. (b) $n = 5$.

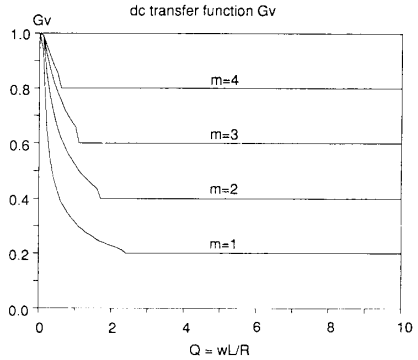

Fig. 10. DC transfer function as function of load and m for $n = 5$.

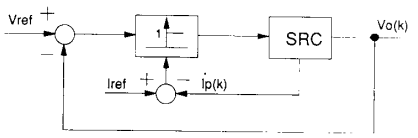

Fig. 11. Block diagram of output voltage feedback control scheme.

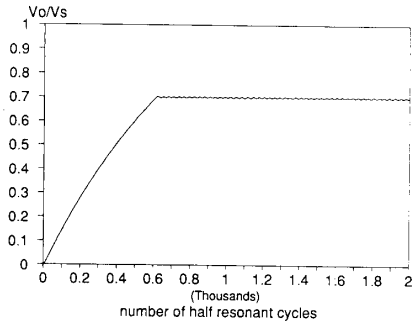

Fig. 12. Simulation result of transient response of normalized dc output voltage waveform (G_v) where $Z = 200\ \Omega$, $\delta = 0.0001$, $Z/R = 5$, $I_{ref} = 10$ A, and $V_{ref}/V_s = 0.7$.

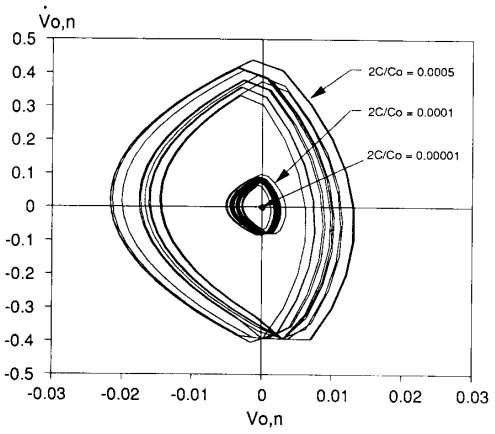

Fig. 13. Diagram of steady state limit cycle on phase plane for normalized output error voltage $V_{o,n}$ where $V_{o,n} = ((V_o - V_{ref})/V_{ref})$.

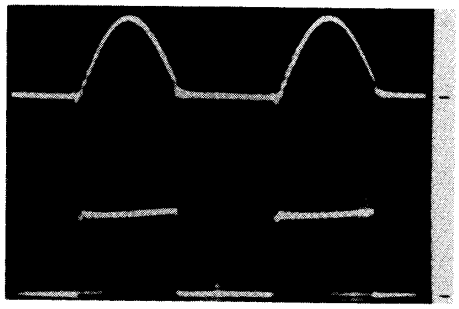

Fig. 14. Waveforms of voltage v_{S2} and current i_{S2} of switch $S2$. Upper trace (v_{S2}): 50 V/div. Lower trace (i_{S2}): 2 A/div. Time scale: 2 μs/div.

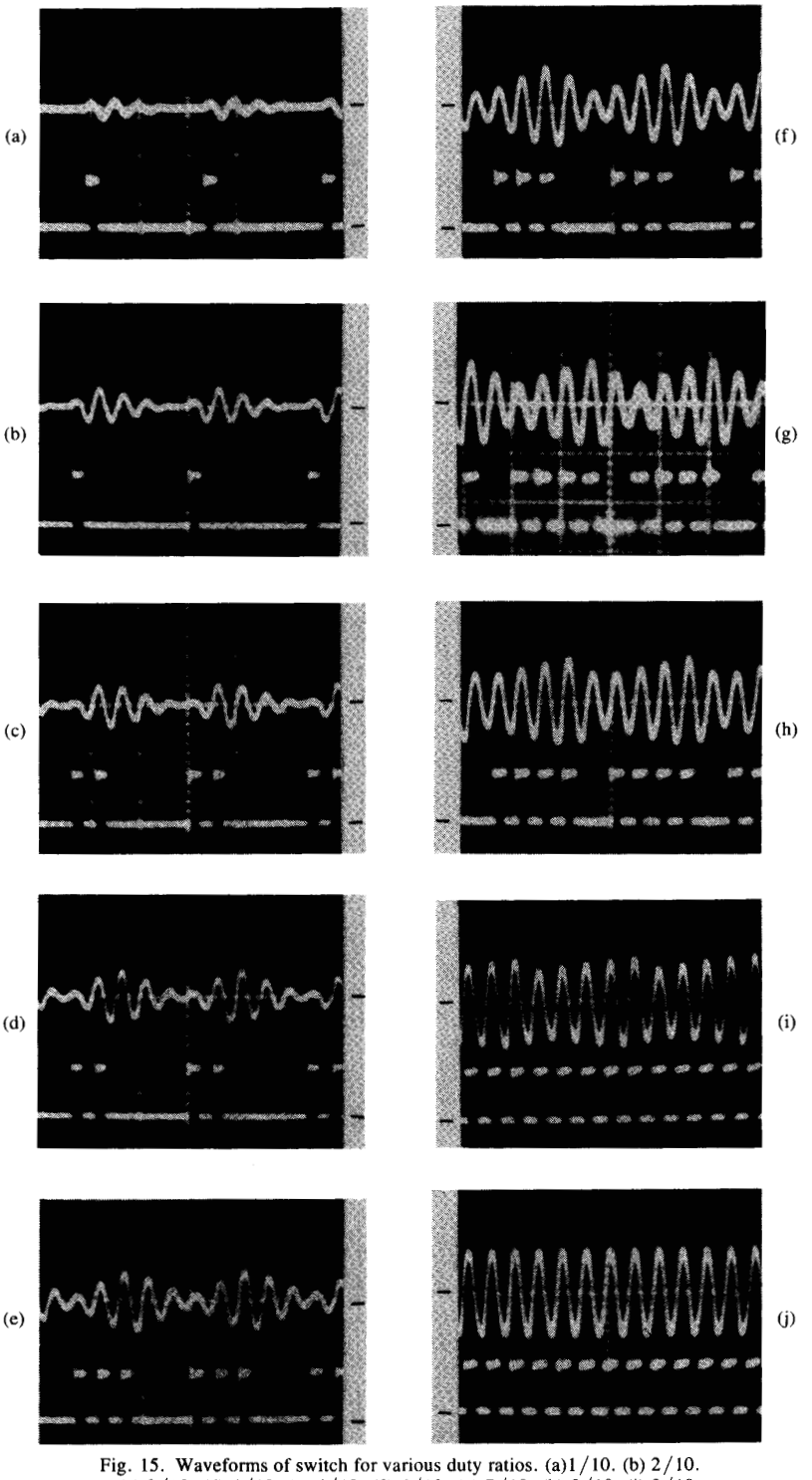

Fig. 15. Waveforms of switch for various duty ratios. (a)1/10. (b) 2/10. (c) 3/10. (d) 4/10. (e) 5/10. (f) 6/10. (g) 7/10. (h) 8/10. (i) 9/10. (j) 10/10. Upper trace (inductor current i_L): 5 A/div. Lower trace (switch voltage v_{S2}): 100 V/div. Time scale: 20 μs/div.

the output voltage and the command voltage. Therefore, the output voltage can be effectively regulated by feedback control. In the miner loop, the peak resonant current is limited to a predetermined value to protect the power device during the powering mode operation. Especially in the transient or load dynamic state, the resonant current can be effectively limited to the predetermined value.

Fig. 12 shows the simulation result of the control dia-

gram when the output voltage command is given as a step function. The output voltage has no overshoot during the transient state and it is regulated during the steady state. The transient response time is functions of filter size, load condition, and reference peak inductor current I_{ref}.

One demerit of such a control scheme is the output voltage ripple during steady-state operation due to the limit cycle phenomenon [10]. Fig. 13 shows the steady-state limit cycle on phase plane. The magnitude of the normalized output error voltage decreases as the capacitance ratio of C and C_o decreases as shown in Fig. 13. This phenomenon occurs because of the low frequency control cycles due to the simple control pattern as shown in Fig. 11. Therefore, such a kind of limit cycle can be reduced further by adapting suitable control pattern or inserting an additional filter at the output side.

IV. Experiments

In this experiment, the full-bridge converter shown in Fig. 1 is used. The converter is designed to have the maximum output power $P_{max} = 250$ W at 100 kHz of operating frequency. The parameter values of the converter are given as follows:

$$L = 258\ \mu\text{H}$$
$$C = 0.0106\ \mu\text{F}$$
$$Z = 156\ \Omega$$
$$C_o = 470\ \mu\text{F}.$$

The voltage and current waveforms flowing on switch S2 are shown in Fig. 14. This oscillogram shows that the switching stress is low because the switching instants are synchronized to the current zero crossing points.

The waveforms of the resonant current and switch voltage are shown in Fig. 15 where the duty ratios are $1/10$, $2/10$, $\cdots$, $10/10$, respectively. These oscillograms show that the powering and free resonant modes are repeated alternately and the switching instants are always synchronized to the current zero crossing points.

Fig. 16 shows the comparison of the measured data and the theoretical values for $n = 10$ and $Q = 1$ ($R = 156\ \Omega$), $Q = 2$ ($R = 78\ \Omega$), and $Q = 5$ ($R = 31.2\ \Omega$), respectively. When $Q = 5$, the theoretical curve with conduction loss compensation has lower gain than the ideal one, as shown in Fig. 16(c), because of the FET series resistance (0.3 Ω), inductor series resistance (0.88 Ω), capacitor series resistance (0.79 Ω), and rectified diode voltage drop (0.6 V). The transformer is eliminated in this experiment. The measured values are nearly coincided with the theoretical values when the conduction losses are considered. In the light load ($Q = 1$ and $Q = 2$) condition, the conduction loss term is small, and the measured values nearly coincide with the theoretical ones, as shown in Fig. 16(a) and (b).

Fig. 17 shows an experimental result of the transient response when the output voltage command is given by a step function. The result shows good regulation with no overshoot.

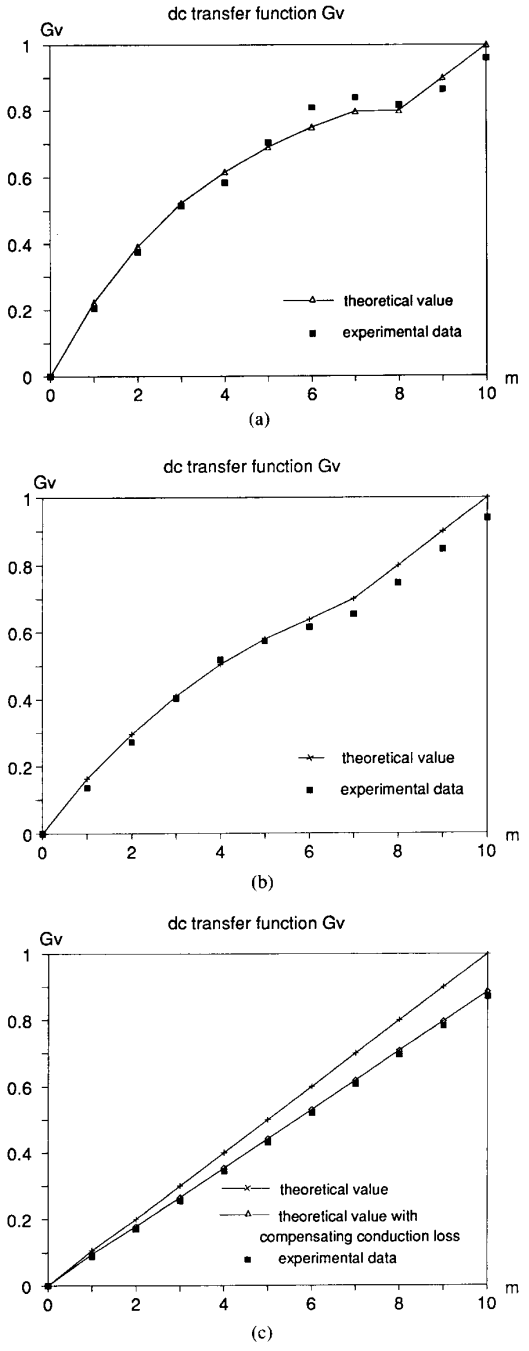

Fig. 16. Comparisons of dc transfer functions between theoretical and experimental results. (a) $Q = 1$ ($R = 156\ \Omega$). (b) $Q = 2$ ($R = 78\ \Omega$). (c) $Q = 5$ ($R = 31.2\ \Omega$).

V. Conclusion

A new control scheme for the SRC is suggested in this paper. The SRC operates at the circuit resonant frequency and the switching instants are always synchronized to the current zero crossing points. Therefore, the major device

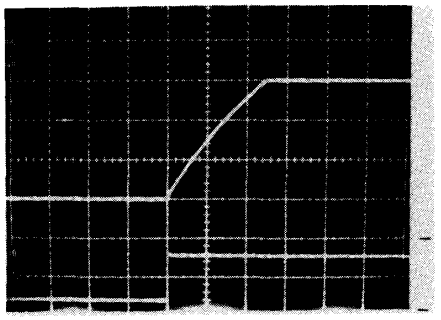

Fig. 17. Transient response of output voltage v_o for command voltage V_{ref}. Upper trace (v_o): 20 V/div. Lower trace: V_{ref}. Time scale: 2 ms/div.

loss is conduction loss and the device capability is fully utilized under high-frequency operation. Converter switching frequency is not limited by the switching loss but by the device turn-on/off time. The output voltage control is achieved by varying the interval length ratio of the switch modes. This control scheme is analyzed in detail, and the characteristics are verified through the experiment. The properties of the proposed scheme are summarized as follows.

1) An SRC always guarantees many advantages, such as zero device switching current, low switching loss, reliable high-frequency operation, and low EMI, because it always operates at optimal condition.

2) For high Q, the dc transfer function is linear to the duty ratio of the powering mode and free resonant mode, and it is independent of the load. Despite a light load condition, the output voltage can be controlled from zero to the maximum.

3) Two demerits of this scheme are discrete output voltage levels and the output voltage ripple due to the limit cycle phenomenon. However, the output voltage can be controlled by feedback scheme, and the output voltage ripple can be reduced further by a suitable control pattern.

Appendix

From Fig. 3, the differential equations of the system for each switch mode are derived as follows.

Powering Mode:

$$\begin{bmatrix} \dot{v}_c^*(t) \\ \dot{i}_L^*(t) \\ \dot{v}_o(t) \end{bmatrix} = \begin{bmatrix} 0 & \frac{1}{C} & 0 \\ -\frac{1}{L} & 0 & -\frac{1}{L} \\ 0 & \frac{1}{C_o} & \frac{-1}{C_oR} \end{bmatrix} \begin{bmatrix} v_c^*(t) \\ i_L^*(t) \\ v_o(t) \end{bmatrix} + \begin{bmatrix} 0 \\ \frac{1}{L} \\ 0 \end{bmatrix} V_s \tag{A1}$$

where

$v_c^*(t) = v_c(t)$ $\quad i_L^*(t) = i_L(t)$ for S1, S4 on

$v_c^*(t) = -v_c(t)$ $\quad i_L^*(t) = -i_L(t)$ for S2, S3 on.

Free Resonant Mode:

$$\begin{bmatrix} \dot{v}_c^*(t) \\ \dot{i}_L^*(t) \\ \dot{v}_o(t) \end{bmatrix} = \begin{bmatrix} 0 & \frac{1}{C} & 0 \\ -\frac{1}{L} & 0 & -\frac{1}{L} \\ 0 & \frac{1}{C_o} & \frac{-1}{C_oR} \end{bmatrix} \begin{bmatrix} v_c^*(t) \\ i_L^*(t) \\ v_o(t) \end{bmatrix} \tag{A2}$$

where

$v_c^*(t) = v_c(t)$ $\quad i_L^*(t) = i_L(t)$ for S4, D2 on

$v_c^*(t) = -v_c(t)$ $\quad i_L^*(t) = -i_L(t)$ for S2, D4 on.

Regeneration Mode:

$$\begin{bmatrix} \dot{v}_c^*(t) \\ \dot{i}_L^*(t) \\ \dot{v}_o(t) \end{bmatrix} = \begin{bmatrix} 0 & \frac{1}{C} & 0 \\ -\frac{1}{L} & 0 & -\frac{1}{L} \\ 0 & \frac{1}{C_o} & \frac{-1}{C_oR} \end{bmatrix} \begin{bmatrix} v_c^*(t) \\ i_L^*(t) \\ v_o(t) \end{bmatrix} + \begin{bmatrix} 0 \\ \frac{-1}{L} \\ 0 \end{bmatrix} V_s \tag{A3}$$

where

$v_c^*(t) = v_c(t)$ $\quad i_L^*(t) = i_L(t)$ for D2, D3 on

$v_c^*(t) = -v_c(t)$ $\quad i_L^*(t) = -i_L(t)$ for D1, D4 on.

Discontinuous Mode:

$$\begin{bmatrix} \dot{v}_c^*(t) \\ \dot{i}_L^*(t) \\ \dot{v}_o(t) \end{bmatrix} = \begin{bmatrix} 0 & 0 & 0 \\ 0 & 0 & 0 \\ 0 & 0 & \frac{-1}{C_oR} \end{bmatrix} \begin{bmatrix} v_c^*(t) \\ i_L^*(t) \\ v_o(t) \end{bmatrix} \tag{A4}$$

where

$v_c^*(t) = v_c(t)$ $\quad i_L^*(t) = i_L(t)$.

References

[1] S. W. H. De Hann, "A new integral pulse module for the series-resonant converter," *IEEE Trans. Ind. Electron.*, vol. IE-31, no. 3, pp. 255-262, Aug. 1984.

[2] R. L. Steigerwald, "High frequency resonant transistor dc-dc converters," *IEEE Trans. Ind. Electron.*, vol. IE-31, no. 2, pp. 181-192, May 1984.

[3] F. C. Schwarz, "An improved method of resonant current pulse modulation for power converters," *IEEE Trans. Ind. Electron., Contr. Intrum.*, vol. IECI-23, no. 2, pp. 133-141, May 1976.

[4] R. J. King and T. A. Stuart, "A large signal dynamic simulation for the series resonant converter," *IEEE Trans. Aerosp. Electron. Syst.*, vol. AES-19, no. 6, pp. 859-870, Nov. 1983.

[5] ——, "Inherent overload protection for the series resonant con-

verter," *IEEE. Trans. Aerosp. Electron. Syst.*, vol. AES-19, no. 6, pp. 820–830, Nov. 1983.
[6] D. M. Divan, "Design considerations for very high frequency resonant mode dc/dc converters," in *Conf. Rec. 1986 IEEE Industry Applications Society Annu. Meeting*, pp. 640–647.
[7] V. Vorperian and S. Cuk, "Small signal analysis of resonant converters," in *Proc. 1983 IEEE PESC Rec.*, pp. 269–282, June 1983.
[8] A. S. Kislovski, "A contribution for steady-state modeling of half-bridge series-resonant power cells," *IEEE Trans. Power Electron.*, vol. PE-1, no. 3, pp. 161–166, July 1986.
[9] I. J. Pitel, "Phase-modulated resonant power conversion techniques for high frequency link inverters," *IEEE Trans. Ind. Appl.*, vol. IA-22, no. 6, pp. 1044–1051, Nov. 1986.
[10] K. J. Kurman, *Feedback Control Theory and Design*. Amsterdam, The Netherlands: Elsevier, 1984.

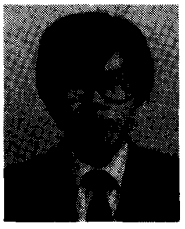

Gyu B. Joung was born in Korea in 1961. He received the B.S. degree from Ajou University, Suwon, Korea, and the M.S. degree from Korea Advanced Institute of Science and Technology (KAIST), Seoul, in 1984 and 1986, respectively, both in electrical engineering. He is presently working towards the Ph.D. degree at KAIST.

His research interests include all aspects of power electronics, particularly resonant converters, and modeling of power converters.

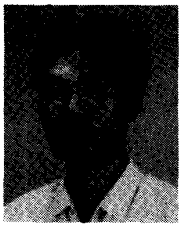

Chun T. Rim was born in Korea on December 7, 1962. He received the B.S. degree from Kumoh Institute of Technology, Kumi, Korea, and the M.S. degree from Korea Advanced Institute of Science and Technology (KAIST), Seoul, in 1985 and 1987, respectively, both in electrical engineering.

He is presently working towards the Ph.D. degree in the same division. His research areas are the modeling of linear switching systems, the control of resonant converters, the design of SMPS and the design of linear IC's.

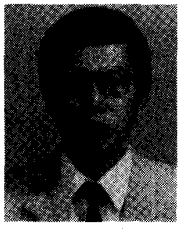

Gyu H. Cho was born in Korea on April 19, 1953. He received the M.S. and Ph.D. degrees from Korea Advanced Institute of Science and Technology (KAIST), Seoul, in 1977 and 1981, respectively.

During 1982–1983, he joined the Electronic Technology Division of Westinghouse R&D Center, Pittsburgh, PA, where he worked on unrestricted frequency changer systems and inverters. Since 1984, he has been an Assistant/Associate Professor in the Electrical Engineering Department of KAIST. His research interests are in the area of static power converters and drives, resonant converters and integrated linear electronic circuit design.